



Multiscale acoustical study on graphene oxide impregnated polyurethane foam

Sung Soo Yang¹ · Inhwa Jung² · Yeon June Kang¹

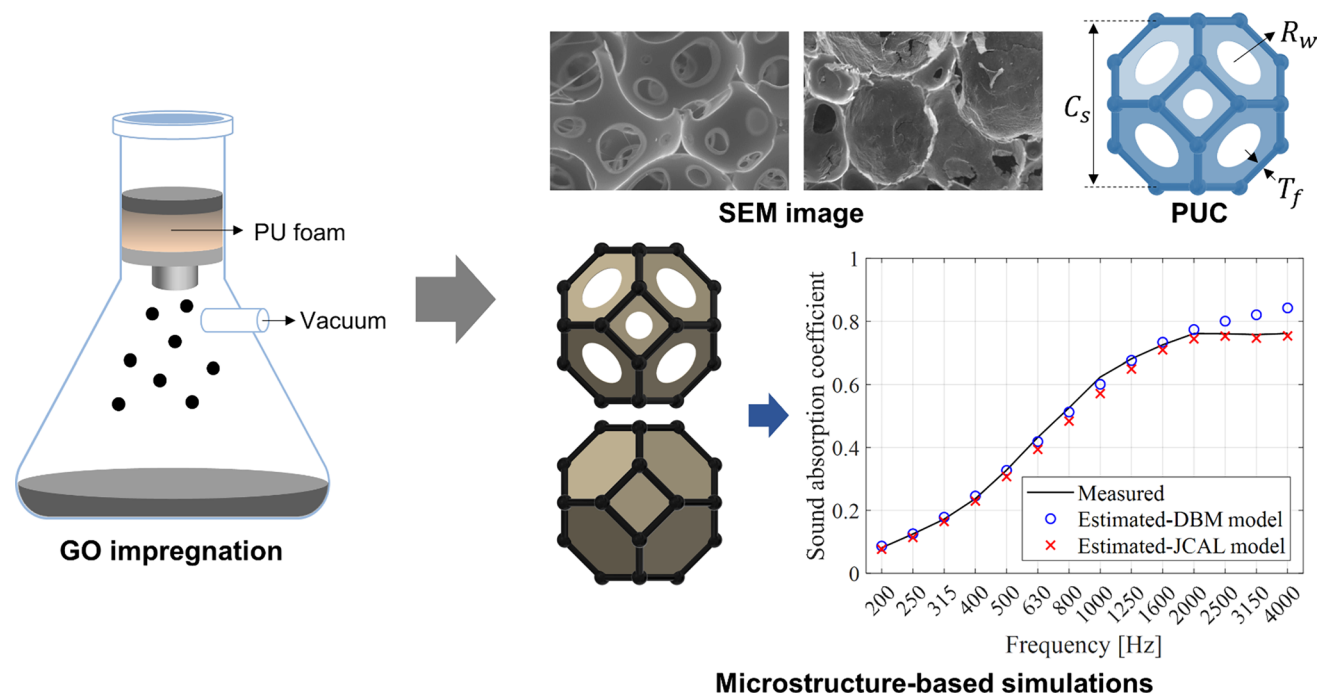
Received: 27 February 2024 / Revised: 6 May 2024 / Accepted: 20 May 2024
© The Author(s), under exclusive licence to The Polymer Society of Korea 2024

Abstract

This study examines the multiscale acoustic properties of sound-absorbing polyurethane (PU) foam impregnated with graphene oxide (GO). GO impregnation into the PU foam was achieved through a vacuum-assisted process. The effects of GO impregnation on the macroscopic acoustic behavior, transport parameters, and sound absorption coefficients were investigated. Scanning electron microscopy images revealed that the impregnated GO enveloped the open pores within the porous structure. Geometric parameters derived from the microstructural observations were used to perform acoustic simulations. Models with partially open cells could be used to accurately predict the transport parameters and sound absorption coefficients of foams with low levels of GO impregnation. For foams with high levels of GO impregnation, it was necessary to incorporate closed cells into the model, which significantly enhanced the prediction accuracy for the transport parameters and sound absorption coefficients. This study advances our understanding of the acoustic properties of GO-impregnated PU foams and will be beneficial for developing more effective sound-absorbing materials.

Graphical abstract

Acoustical characterization of graphene oxide impregnated polyurethane foam



Keywords Graphene oxide · Microstructure · Polyurethane foam · Sound absorption · Transport parameter

Extended author information available on the last page of the article

1 Introduction

Polyurethane (PU) foam effectively dissipates acoustic energy owing to its porous structure with intertwined solid and fluid phases. Consequently, it is utilized for passive noise control in diverse industries, including the automotive, construction, and aviation sectors. Extensive research has been conducted to model the energy dissipation phenomena and elucidate the macroscopic acoustic behavior of PU foams. Delany and Bazley [1] introduced an empirical formula for predicting the acoustic impedance and wavenumber of porous materials, which was subsequently modified by Miki [2]. This formula is efficient because it relies on a single transport parameter (static airflow resistivity). Johnson et al. [3] and Champoux and Allard [4] developed a semi-phenomenological model for predicting the acoustic characteristics of porous materials with arbitrary pore shapes, under the assumption that the solid phase remains stationary. Unlike Delany and Bazley's formula, this model incorporates multiple transport parameters, including open porosity, tortuosity, viscous characteristic length, and thermal characteristic length. Lafarge et al. [5] later refined this model to include static thermal permeability, which significantly enhanced its accuracy in predicting low-frequency behavior.

Numerous studies have focused on improving the acoustic performance of porous materials. Gwon et al. [6] explored the relationship between the microstructure of PU foam and its sound absorption properties, and reported that modifications in the chemical composition or cell structure of PU foam could enhance its sound absorption capabilities. The sound absorption performance of PU foam can also be improved by incorporating carbon nanotubes [7], solid particles [8], aerogels [9], and other fillers [10]. A promising approach involves impregnation with graphene oxide (GO) [11–15]; the impregnated GO envelops the open pores, converting them into closed pores. This transformation complicates the acoustic pathways, resulting in increased viscous and thermal energy dissipation, thereby enhancing the sound absorption behavior [12, 13].

These alterations in the acoustic properties of PU foam can be explained from a microstructural standpoint. However, prior research on GO-impregnated PU foam has predominantly focused on the macroscopic acoustic behavior. In particular, calculating the transport parameters and absorption coefficients from the microstructure has not been sufficiently investigated. Therefore, in this study, we examined the multiscale acoustic characteristics of GO-impregnated PU foam, including its microstructure and macroscopic sound absorption behavior. GO impregnation was performed using a vacuum-assisted process and verified using Raman spectroscopy and scanning electron

microscopy (SEM). Geometric parameters were derived from the microstructural data and used to model a periodic unit cell (PUC) structure resembling a Kelvin cell, wherein the opening ratio of the cell was modified by GO impregnation. The simulated transport parameters were compared with the experimental values to assess the prediction accuracy of the model. Additionally, the sound absorption coefficients, predicted using a rigid-frame porous model, were compared with those obtained using an impedance tube. The results demonstrate that the change in the macroscopic acoustic behavior of PU foam resulting from GO impregnation can be predicted from its microstructural characteristics. This research deepens our understanding of the multiscale acoustic characteristics of GO-impregnated PU foam and provides a foundation for the development of more effective sound-absorbing materials for noise-control applications.

2 Multiscale acoustical description of sound-absorbing porous materials

2.1 Microscopic approach

The macroscopic visco-inertial and thermal energy dissipation properties of porous materials are closely related to their microstructures. PU foam features a cellular structure with interconnected pores, which can be approximated as an ideal PUC structure. Typical PUC structures include simple cubic, body-centered cubic, and face-centered cubic configurations. In this study, we utilized the Kelvin cell structure, which is suitable for modeling the microstructure of foams with high open porosity. Figure 1 depicts typical Kelvin cell structures with fully open, partially open, and fully closed cell configurations. The type of Kelvin cell depends on the membrane structure in the observed material. To construct a Kelvin cell structure, three microstructural parameters must be determined (Fig. 2): cell size (C_s), strut thickness (T_f), and opening ratio (R_w). These parameters can be determined from SEM or micro-computed tomography images using image processing techniques [16]. Once the PUC structure is established, the transport parameters can be computed through

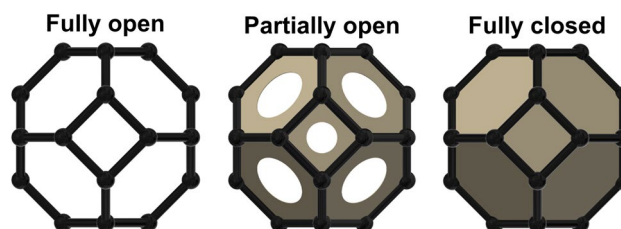


Fig. 1 Kelvin cell structures with fully open, partially open, and fully closed configurations

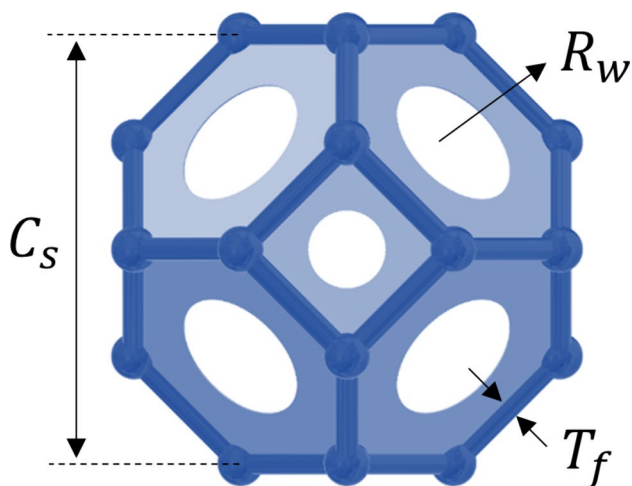


Fig. 2 Geometrical parameters of Kelvin cell structure

microstructure-based numerical calculations. The open porosity (ϕ), which indicates the volumetric ratio of the fluid phase to the total material, can be readily calculated from the PUC structure. Other transport parameters (e.g., static airflow resistivity, tortuosity, viscous characteristic length, thermal characteristic length, and static thermal permeability) can be derived from microstructure-based simulations, as described below.

2.1.1 Stokes problem

The static airflow resistivity (σ), characterizing visco-inertial effects at low frequencies, can be obtained by solving the Stokes problem. Low-Reynolds number flows (creeping flows) can be expressed as a Stokes problem with the following boundary conditions [17]:

$$\mu \nabla^2 \mathbf{v} - \nabla p = \mathbf{g} \text{ in } \Omega_f, \tag{1}$$

$$\nabla \cdot \mathbf{v} = 0 \text{ in } \Omega_f, \tag{2}$$

$$\mathbf{v} = 0 \text{ on } \Omega_{sf}, \tag{3}$$

where μ , \mathbf{v} , p , \mathbf{g} , Ω_f , and Ω_{sf} represent the dynamic viscosity of air, velocity field of the fluid, pressure of the fluid, pressure gradient acting as a forcing term, fluid domain, and solid–fluid interface domain, respectively. The static airflow resistivity can be calculated as $\sigma = \mu / \phi \langle k_0 \rangle$ by solving Eqs. (1–3) in the fluid domain, where $k_0 = -\mu \mathbf{v} / \mathbf{g}$ denotes the static viscous permeability.

2.1.2 Laplace problem

In high-frequency regimes, the fluid behavior becomes inviscid. The influence of viscous forces can be neglected as the

Reynolds number approaches infinity. Moreover, such inviscid flow can be analogously represented by electrical conduction (Laplace problem) simulations, applying the following boundary conditions [17]:

$$\mathbf{E} = -\nabla \varphi + \mathbf{e} \text{ in } \Omega_f, \tag{4}$$

$$\nabla \cdot \mathbf{E} = 0 \text{ in } \Omega_f, \tag{5}$$

$$\mathbf{E} \cdot \mathbf{n} = 0 \text{ on } \Omega_{sf}, \tag{6}$$

where \mathbf{E} , φ , \mathbf{e} , and \mathbf{n} denote the electric field, electric potential, unit vector field, and unit vector normal to the solid–fluid interface, respectively. The tortuosity (τ), viscous characteristic length (Λ), and thermal characteristic length (Λ') can be derived by solving Eqs. (4–6) in the fluid domain as follows. Tortuosity, which accounts for visco-inertial effects at high frequencies, can be calculated as $\tau = \langle \mathbf{E}^2 \rangle / \langle \mathbf{e}^2 \rangle$. The viscous characteristic length, representing the viscous effects at high frequencies, can be computed as $\Lambda = 2 \left(\int_{\Omega_f} \mathbf{E}^2 d\Omega_f \right) / \left(\int_{\Omega_{sf}} \mathbf{E}^2 d\Omega_{sf} \right)$. The thermal characteristic length, a geometrical parameter related to thermal effects at high frequencies, and can be obtained as $\Lambda' = 2 \left| \Omega_f \right| / \left| \Omega_{sf} \right|$.

2.1.3 Poisson problem

The static thermal permeability (k'_0) is a geometrical parameter that describes the thermal exchange between the solid and fluid phases. It can be calculated by conducting a heat diffusion simulation (Poisson problem) with the following boundary conditions [17]:

$$\nabla^2 \theta = -1 \text{ in } \Omega_f, \tag{7}$$

$$\theta = 0 \text{ on } \Omega_{sf}, \tag{8}$$

where θ is the temperature field. k'_0 has the dimension of a surface, and can be computed as $k'_0 = \phi \langle \theta \rangle$. Note that k'_0 is associated with the low-frequency behavior of thermal effects.

2.2 Macroscopic approach

Porous materials dissipate acoustic energy through visco-inertial and thermal effects, which can be modeled based on the intrinsic transport parameters of the material. The normal incident sound absorption coefficient α of single porous layer can be calculated as follows:

$$\alpha(\omega) = 1 - \left| \frac{Z_s - Z_0}{Z_s + Z_0} \right|^2, \tag{9}$$

where Z_s and Z_0 represent the surface impedance of the porous material and the characteristic impedance of air, respectively. Subsequently, Z_s can be computed as follows:

$$Z_s(\omega) = -jZ_c \cot(kL), \quad (10)$$

where Z_c , k , and L denote the characteristic impedance, complex wavenumber, and porous-layer thickness, respectively. Consequently, the macroscopic sound absorption behavior of porous materials can be predicted by calculating Z_c and k using the transport parameters. The Delany–Bazley–Miki (DBM) model, a commonly used empirical formula, employs static airflow resistivity as the sole input parameter. According to the DBM model, Z_c and k can be expressed as follows [1, 2]:

$$Z_c(\omega) = \rho_0 c \left[1 + 5.50 \left(10^3 \frac{f}{\sigma} \right)^{-0.632} - j8.43 \left(10^3 \frac{f}{\sigma} \right)^{-0.632} \right], \quad (11)$$

$$k(\omega) = \frac{\omega}{c} \left[1 + 7.81 \left(10^3 \frac{f}{\sigma} \right)^{-0.618} - j11.41 \left(10^3 \frac{f}{\sigma} \right)^{-0.618} \right], \quad (12)$$

where ρ_0 and c represent the density and speed of sound in air, respectively. The Johnson–Champoux–Allard–Lafarge (JCAL) model is an alternative model based on semi-phenomenological relationships. Assuming that the solid phase of the porous material remains stationary, Z_c and k can be expressed as follows:

$$Z_c(\omega) = \sqrt{\rho_{eff} \times K_{eff}}, \quad (13)$$

$$k(\omega) = \omega \sqrt{\rho_{eff} / K_{eff}}, \quad (14)$$

where ρ_{eff} and K_{eff} denote the effective mass density and effective bulk modulus, respectively. According to the JCAL model, for a porous structure with a motionless skeleton and arbitrary pore shapes, ρ_{eff} and K_{eff} are expressed as follows [3–5]:

$$\rho_{eff}(\omega) = \frac{\tau \rho_0}{\phi} \left[1 + \frac{\sigma \phi}{j\omega \rho_0 \tau} \sqrt{1 + j \frac{4\tau^2 \eta \rho_0 \omega}{\sigma^2 \Lambda^2 \phi^2}} \right], \quad (15)$$

$$K_{eff}(\omega) = \frac{\gamma P_0 / \phi}{\gamma - (\gamma - 1) \left[1 - j \frac{\phi \kappa}{k'_0 C_p \rho_0 \omega} \sqrt{1 + j \frac{4k'_0{}^2 C_p \rho_0 \omega}{\kappa \Lambda^2 \phi^2}} \right]^{-1}}, \quad (16)$$

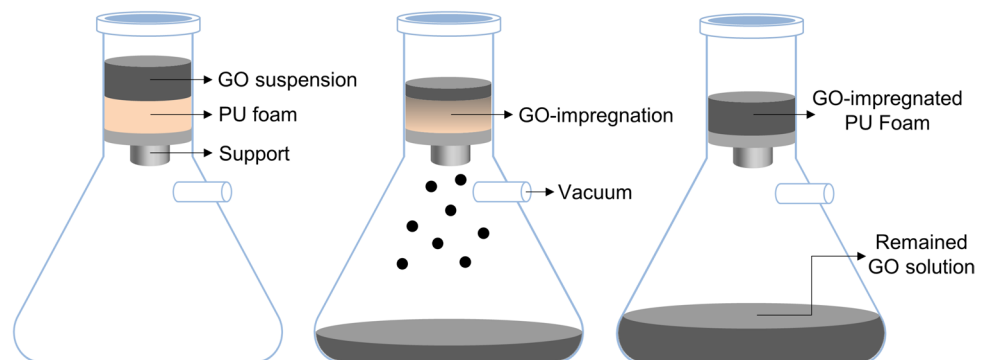
where η , γ , C_p , and κ represent the dynamic viscosity, specific heat ratio, specific heat at constant pressure, and thermal conductivity of air, respectively. Unlike the DBM model, the JCAL model requires six transport parameters for predicting the macroscopic sound absorption behavior of porous materials.

3 Experimental

3.1 Graphene oxide-impregnation of polyurethane foam

The vacuum-assisted method for impregnating PU foam with GO is shown schematically in Fig. 3. We used commercially available sound-absorbing PU foam (NVH KOREA Inc., Republic of Korea) and an aqueous GO solution (2 wt% GO; N002-PS, Angstrom Materials, USA) diluted by a factor of 5. The pristine PU foam was flexible with a partially open cell structure, and the individual GO particles had an average lateral size and thickness of 554 and 1.2 nm, respectively. Pristine PU foam samples measuring $\varnothing 100 \times 20$ mm were subjected to 1–4 GO impregnation cycles to modify the GO content. For each impregnation cycle, the PU foam was placed in the neck of a flask on a support, and then 200 mL of GO solution was poured on top of and flowed through the foam. The use of vacuum pressure enhanced the impregnation rate while minimizing damage to the pore structure [12]. The foam samples were thoroughly dried for 48 h at 20 °C between each impregnation cycle.

Fig. 3 Process of GO impregnation into PU foam



3.2 Characterization of transport parameters and sound absorption coefficient

The open porosity of the PU foams was determined using a porosity meter (PHI, Mecanum Inc., Canada), employing the pressure/mass method [18]. Tortuosity was measured using a tortuosity meter (TOR, Mecanum Inc., Canada) through the ultrasonic method [19]. Static airflow resistivity was assessed using a custom device according to ASTM C522-03 [20]. Other transport parameters were measured on samples with diameters of 100 mm. The remaining three transport parameters (Λ , Λ' , and k'_0) were quantified indirectly [21] using an impedance tube (Type-4206, Brüel and Kjær, Denmark) with a four-microphone configuration (Fig. 4) and PU foam samples with diameters of 29 mm. The impedance tube was additionally utilized to measure the normal incident sound absorption coefficient of PU foams, coupled with a microphone pair (Type-4187, Brüel and Kjær, Denmark), data acquisition system (LMS SCADAS mobile, Siemens, Germany), and software (Simcenter Testlab, Siemens, Germany). For these measurements, the PU foam was rigidly backed within the tube, and a two-microphone configuration (Fig. 4) was used to determine the absorption coefficient.

4 Results and discussion

4.1 Multiscale acoustical analysis of pristine PU foam

Prior to investigating the GO-impregnated PU foam, we conducted a detailed multiscale acoustic analysis of the pristine PU foam. The microstructure, as observed by SEM, is depicted in Fig. 5.

The microstructural parameters were quantified following the process in Sect. 2.1 and used to construct a Kelvin cell-type PUC. The C_s , T_f , and R_w values were 420 μm , 55 μm , and 51%, respectively. As shown in Fig. 5, the cell

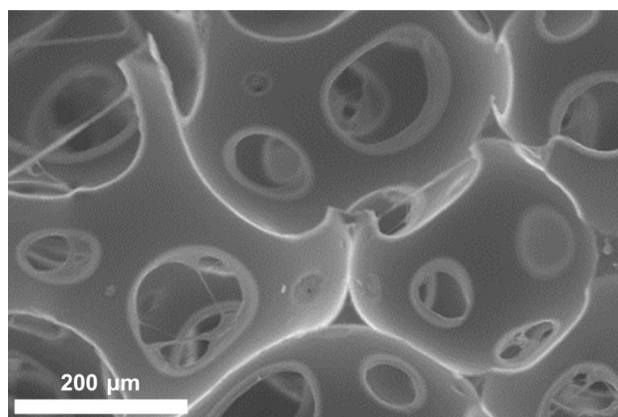
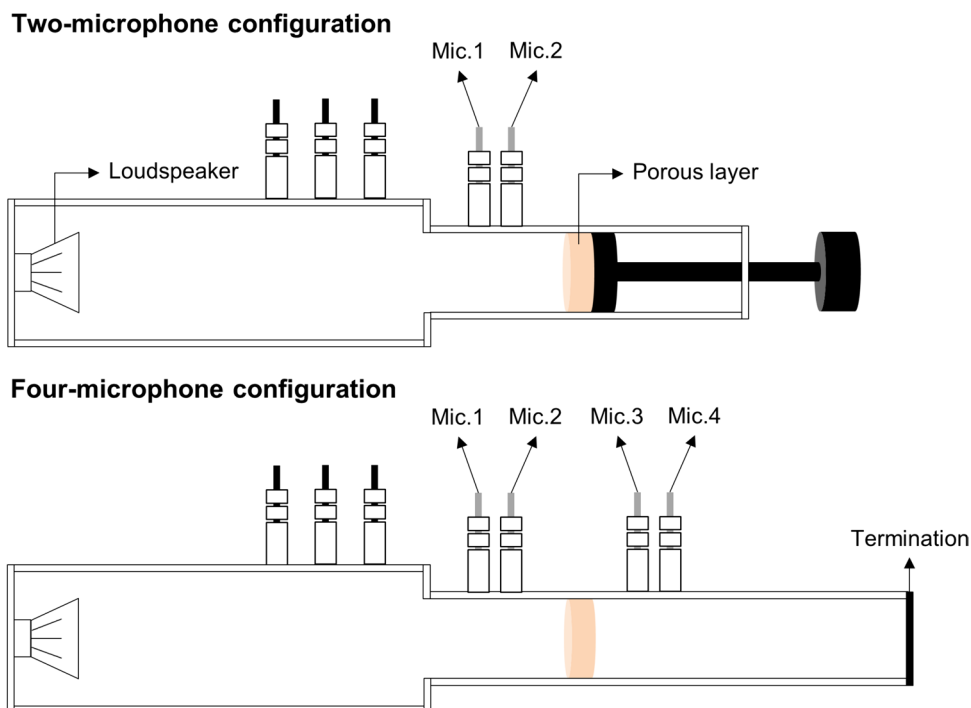


Fig. 5 SEM image of pristine PU foam

Fig. 4 Schematic of impedance tube measurements



structure exhibited a partially open configuration. Therefore, the PUC was modeled to reflect a partially open cell configuration (Fig. 1). The transport parameters were computed using Eqs. (1–8) based on the constructed PUC, and the calculated values were compared with the experimental results (Table 1). All six microstructure-derived transport parameters closely matched the measured values, indicating that modeling with a partially open Kelvin cell configuration is effective for predicting the macroscopic transport parameters of pristine PU foam.

The normal incident sound absorption coefficients of the pristine PU foam were predicted using the DBM and JCAL models based on the measured and calculated transport parameters (Table 1) and compared with the experimental values (Fig. 6). The measured and calculated transport parameters both demonstrated high predictive accuracy for the absorption coefficient. Moreover, the DBM and JCAL models were both effective for characterizing the macroscopic acoustic behavior of the pristine PU foam.

Table 1 Macroscopic transport parameters of pristine PU foam

Transport parameters	Measured	Calculated (percent error)
ϕ [-]	0.891	0.890 (-0.11%)
τ [-]	1.27	1.25 (-1.57%)
σ [$\times 10^3$ rayl/m]	22.3	21.9 (-1.79%)
Λ [μm]	80.0	80.1 (+0.12%)
Λ' [μm]	165	164 (-0.61%)
k'_0 [$\times 10^{-10}$ m ²]	30.0	30.2 (+0.67%)

The calculated values were derived from a model with a partially open cell configuration

4.2 Multiscale acoustical analysis of GO-impregnated PU foam

We next explored the multiscale acoustic characteristics of GO-impregnated PU foams after 1–4 cycles of impregnation (denoted as GO1–GO4, respectively). The color changed from white to black with successive impregnation cycles (Fig. 7). Figure 8 shows the GO contents of each sample. On average, 3.3 wt% GO was incorporated into the PU foam per cycle. The presence of impregnated GO in the PU foam was verified using Raman spectroscopy, performed with a spectrometer (DXR2, Thermo Fisher Scientific Inc., USA). Raman spectra of the pristine PU foam and GO4 samples are presented in Fig. 9. The Raman spectrum of the pristine PU foam contained peaks corresponding to CH₃ stretching (2974 cm⁻¹), CH₂ stretching (2933 and 2871 cm⁻¹), C=C stretching (1615 cm⁻¹), CH₂ bending (1454 cm⁻¹), CH₂

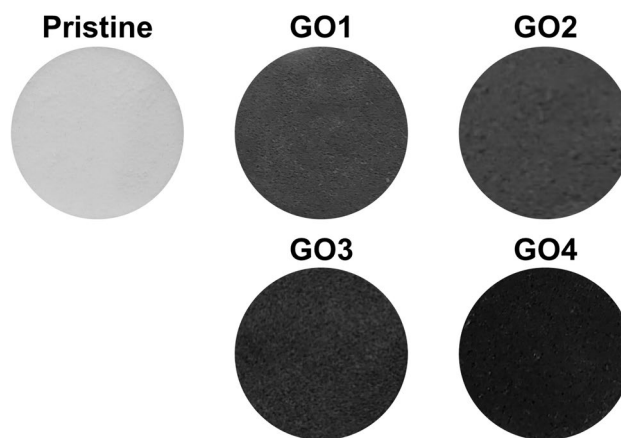


Fig. 7 Images of pristine and GO-impregnated PU foam samples

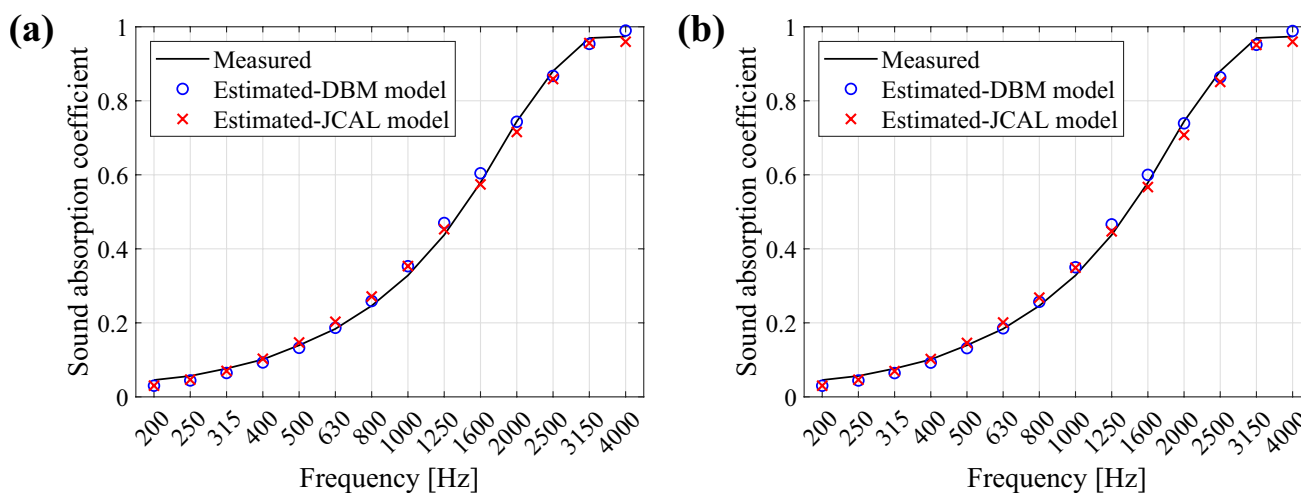


Fig. 6 Sound absorption coefficients of pristine PU foam predicted by DBM and JCAL models using **a** measured and **b** calculated transport parameters; the experimental values are shown for comparison

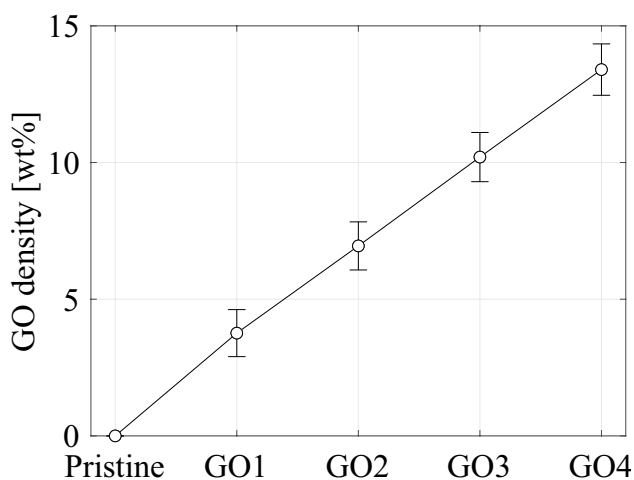


Fig. 8 GO content of PU foam relative to number of impregnation cycles

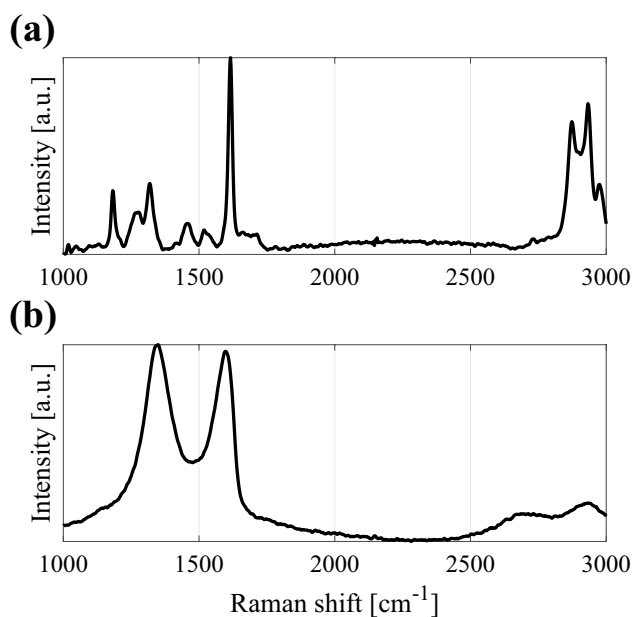


Fig. 9 Raman spectra of **a** pristine PU foam and **b** GO4

wag/twist (1319 cm^{-1}), and C–O stretching (1184 cm^{-1}) [22]. Significant changes in the Raman spectrum of GO4 were observed owing to GO impregnation. Specifically, two peaks characteristic of GO, associated with the G band (1597 cm^{-1}) and D band (1357 cm^{-1}), were identified [12].

SEM images of GO1 and GO4 are shown in Fig. 10a and b, respectively. Compared to the pristine PU foam (Fig. 5), the GO-impregnated samples had fewer open pores, indicating that the GO flakes cover the open pores. For GO1, the cell structure remained partially open, akin to that of the pristine PU foam, but with a reduced opening ratio. Similarly, GO4 demonstrated a decreased cell-opening ratio, with

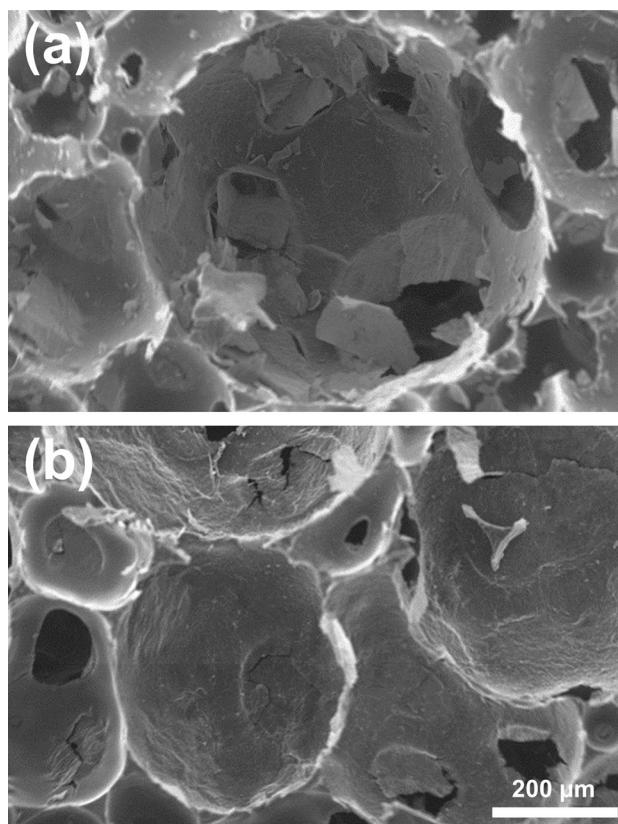


Fig. 10 SEM images of GO-impregnated PU foams: **a** GO1 and **b** GO4

a higher proportion of fully closed windows owing to the increased GO content. The microstructural parameters of GO1–GO4 were determined from the SEM images. Since the cell size and strut thickness were minimally affected by GO impregnation, C_s and T_f were presumed to be the same as those of the pristine PU foam (420 and $55\text{ }\mu\text{m}$, respectively); therefore, only the opening ratio (R_w) was measured. The R_w values for GO1–GO4 were 34%, 28%, 22%, and 16%, respectively, signifying a substantial decrease compared to that of the pristine PU foam ($R_w = 51\%$). Kelvin cell-type PUCs were constructed for each sample based on the derived microstructural parameters. The initial modeling approach treated all samples as having partially open cells. The transport parameters were calculated for each modeled Kelvin cell using Eqs. (1–8), and compared with the measured values (Table 2).

Since the PUCs of GO1–GO4 were all modeled as partially open cells, the calculated open porosity was the same for all samples, regardless of the R_w value. However, as indicated in Table 2, the measured open porosity decreased with increasing GO content. In addition, the measured values were all lower than that of the pristine PU foam (Table 1). This resulted in a growing discrepancy between the calculated and measured values with successive impregnation

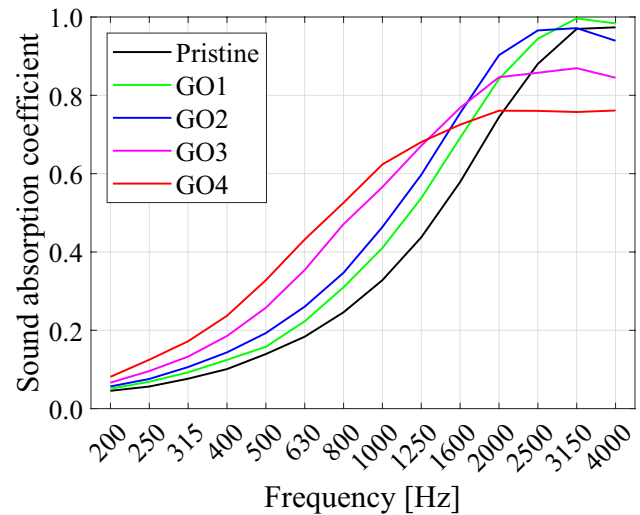
Table 2 Transport parameters of GO-impregnated PU foams

Transport parameter	Measured	Calculated (percent error)
ϕ [-]	GO1: 0.876	GO1: 0.890 (+1.60%)
	GO2: 0.858	GO2: 0.890 (+3.73%)
	GO3: 0.845	GO3: 0.890 (+5.33%)
	GO4: 0.819	GO4: 0.890 (+8.67%)
τ [-]	GO1: 1.32	GO1: 1.38 (+4.55%)
	GO2: 1.56	GO2: 1.50 (-3.85%)
	GO3: 1.70	GO3: 1.66 (-2.35%)
	GO4: 2.19	GO4: 1.90 (-13.24%)
σ [$\times 10^3$ rayl/m]	GO1: 30.3	GO1: 32.4 (+6.93%)
	GO2: 46.2	GO2: 42.2 (-8.66%)
	GO3: 77.8	GO3: 71.1 (-8.61%)
	GO4: 119	GO4: 100 (-15.97%)
Λ [μm]	GO1: 71.0	GO1: 69.6 (-1.97%)
	GO2: 66.0	GO2: 65.7 (-0.45%)
	GO3: 60.0	GO3: 63.2 (+5.33%)
	GO4: 40.0	GO4: 52.2 (+30.5%)
Λ' [μm]	GO1: 151	GO1: 150 (-0.66%)
	GO2: 135	GO2: 142 (+5.19%)
	GO3: 120	GO3: 131 (+9.17%)
	GO4: 109	GO4: 120 (+10.09%)
k'_0 [$\times 10^{-10}$ m ²]	GO1: 28.0	GO1: 28.5 (+1.79%)
	GO2: 26.0	GO2: 27.6 (+6.15%)
	GO3: 25.0	GO3: 26.4 (+5.60%)
	GO4: 23.0	GO4: 25.1 (+9.13%)

The calculated values were derived from models with a partially open cell configuration

cycles. This phenomenon likely arises from an increase in the number of dead-end and fully closed cells. For GO1–GO3, the prediction accuracy for tortuosity and static airflow resistivity was high. However, significant errors were observed for the heavily impregnated GO4. Along with the open porosity, the tortuosity significantly influences the high-frequency sound absorption coefficient, potentially compromising the prediction accuracy. While the prediction errors for the static thermal permeability were relatively small for all samples, those for the viscous and thermal characteristic lengths increased with increasing GO content.

Figure 11 shows the macroscopic sound absorption behavior of the pristine and GO-impregnated PU foams. In the low-frequency range (< 1250 Hz), the sound absorption coefficient increased significantly with increasing GO content. This is attributed to the increase in static airflow resistivity, which greatly influences the low-frequency absorption coefficient, as well as the increased complexity of the acoustic path stemming from the reduction in open porosity [12]. In comparison to pristine PU foam, GO1 exhibited enhanced sound absorption performance across the entire frequency range, whereas GO2–GO4

**Fig. 11** Measured sound absorption coefficients of pristine and GO-impregnated PU foams

exhibited reduced absorption coefficients in the high-frequency range. In particular, the absorption coefficient of the heavily impregnated GO4 was lower than those of the less impregnated foams at frequencies above ~1600 Hz and lower than that of pristine PU foam at frequencies exceeding 2000 Hz. This phenomenon arises because of the increase in static airflow resistivity, which shifts the maximum absorption coefficient toward lower frequencies. Therefore, in applications where high-frequency sound absorption performance is crucial, excessive GO impregnation may harm the acoustic performance of PU foam.

The absorption coefficients of the GO-impregnated foams were predicted using the DBM and JCAL models based on the measured and calculated transport parameters listed in Table 2, and compared with the experimental values shown in Fig. 11. The results for GO1–GO4 are shown in Figs. 12–15, respectively. For GO1 and GO2 (Figs. 12 and 13, respectively), the absorption coefficients predicted from the measured and calculated transport parameters demonstrated excellent agreement with the experimental values using both the DBM and JCAL models. Thus, both models have high prediction accuracies for the macroscopic sound absorption behavior of GO1 and GO2. For GO3 (Fig. 14), the predicted values were in close alignment with the experimental values; however, a slight decrease in prediction accuracy was observed at high frequencies when using the calculated transport parameters. This trend was even more pronounced for GO4 (Fig. 15), which contained the highest GO content. Moreover, the prediction accuracy of the DBM model for GO4 was low even when using measured transport parameters. This is because the DBM model relies solely on the static airflow resistivity as its input variable. By contrast, the JCAL

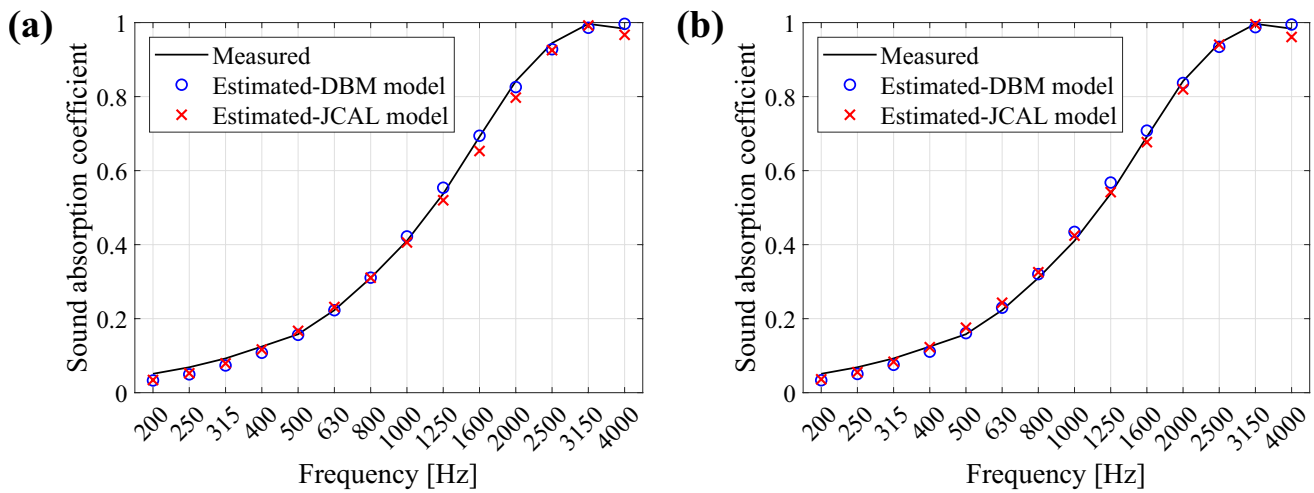


Fig. 12 Sound absorption coefficients of GO1 predicted by DBM and JCAL models using **a** measured and **b** calculated transport parameters; the experimental values are shown for comparison

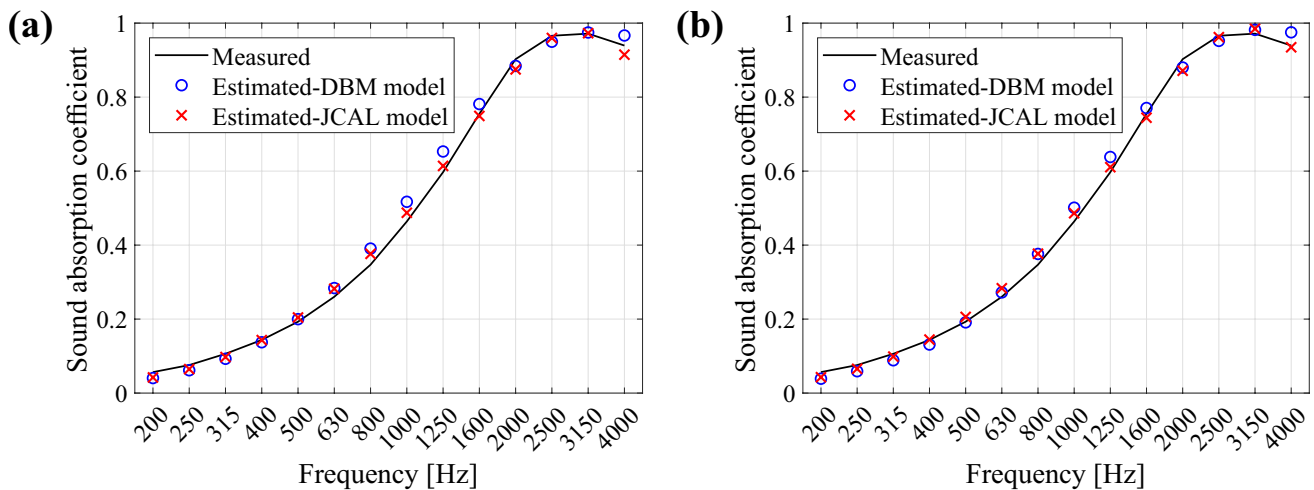


Fig. 13 Sound absorption coefficients of GO2 predicted by DBM and JCAL models using **a** measured and **b** calculated transport parameters; the experimental values are shown for comparison

model, which utilizes six transport parameters, typically achieves higher prediction accuracy.

The diminished absorption coefficient prediction ability for GO4 arises from the inability to accurately predict the transport parameters, as shown in Table 2. As shown in Fig. 10, GO4 contained an increase proportion of fully closed windows. Therefore, this limitation stems from modeling the microstructure using partially open cells. Specifically, the partially open-cell model cannot reflect the decrease in open porosity caused by closed and dead-end pores (Fig. 10). To examine the effect of fully closed cells, a PUC model was developed with both partially open and fully closed windows. The Kelvin cell comprises six square and eight hexagonal faces. Therefore, using random number generation [23], specific cell walls were modeled as fully

closed windows, whereas the remaining ones were configured as partially open windows. For instance, a cell with an opening ratio of 15% may be modeled by rendering four square-shaped faces and six hexagonal faces as fully closed windows, with the remaining faces as fully open windows [23]. Consequently, for GO4, which had an opening ratio of 16%, four square-shaped faces and four hexagonal faces were treated as fully closed windows, and the remaining faces were modeled as partially open windows. The transport parameters of the GO4 sample, calculated based on the Kelvin cell-type PUC incorporating fully closed windows, are listed in Table 3.

As illustrated in Table 2, the model with only partially open cells failed to simulate the reduction in open porosity caused by GO impregnation. By contrast, the model

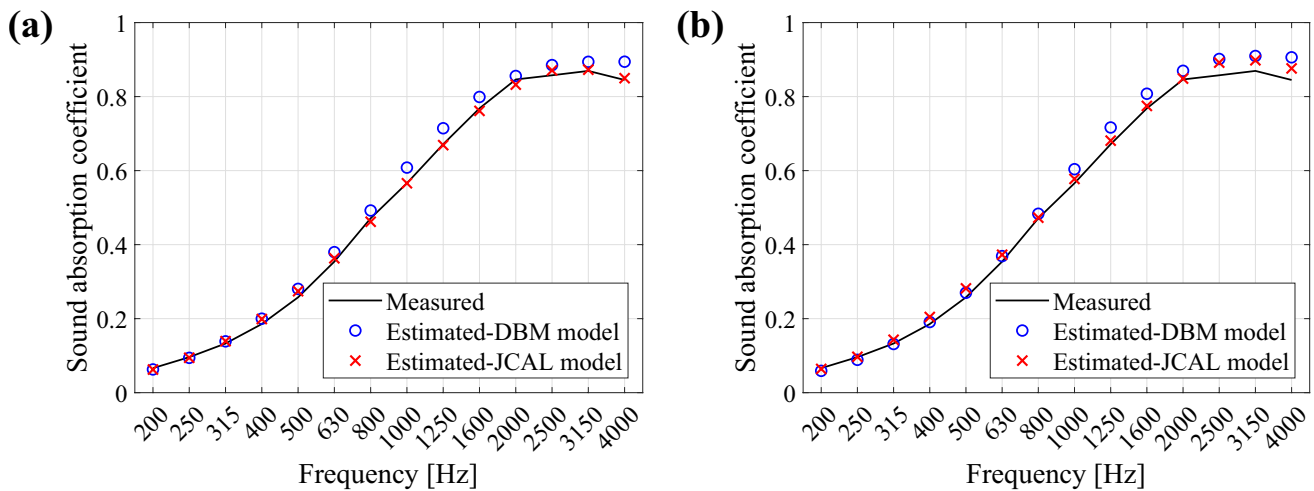


Fig. 14 Sound absorption coefficients of GO3 predicted by DBM and JCAL models using **a** measured and **b** calculated transport parameters; the experimental values are shown for comparison

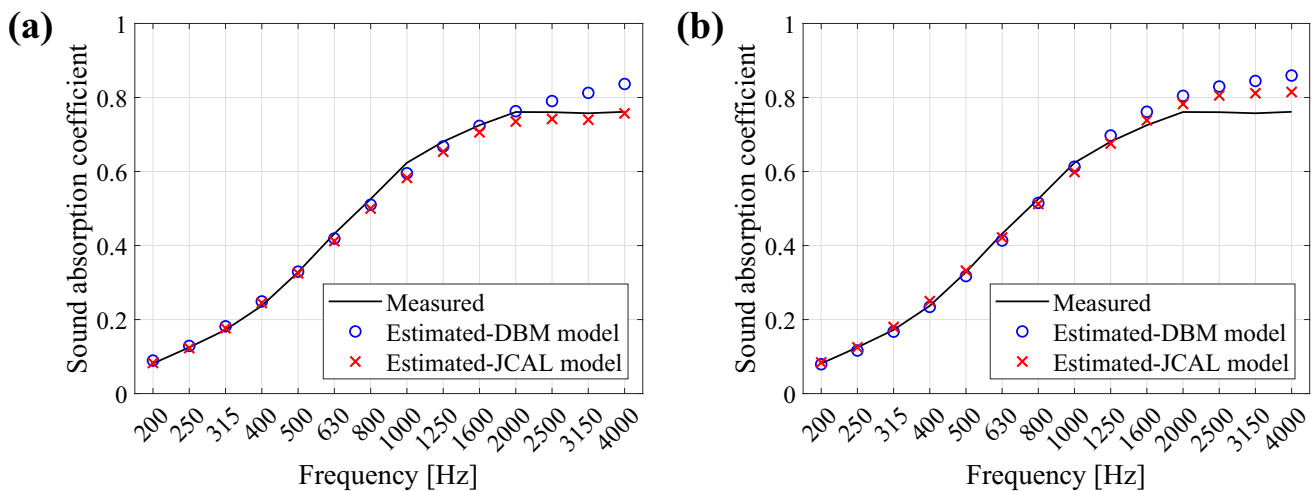


Fig. 15 Sound absorption coefficients of GO4 predicted by DBM and JCAL models using **a** measured and **b** calculated transport parameters; the experimental values are shown for comparison

Table 3 Transport parameters of GO4

Transport parameters	Measured	Calculated (percent error)
ϕ [-]	0.819	0.790 (-3.54%)
τ [-]	2.19	2.06 (-5.94%)
σ [$\times 10^3$ rayl/m]	119	114 (-4.20%)
Λ [μm]	40.0	41.4 (+3.50%)
Λ' [μm]	109	115 (+5.50%)
k'_0 [$\times 10^{-10}$ m ²]	23.0	23.8 (+3.48%)

The calculated values were derived from a model incorporating fully closed windows

combining both partially open and fully closed windows more successfully replicated this reduction. The prediction accuracy of the other transport parameters also improved. The absorption coefficient of the GO4 sample was predicted by the DBM and JCAL models using the newly calculated transport parameters, as shown in Fig. 16. Notably, the consistency in predicting the acoustic behavior using the JCAL model was significantly improved compared to that shown in Fig. 15. The values predicted using the DBM model were still less accurate owing to the use of a single input parameter (static airflow resistivity); therefore, the DBM model is not suitable for predicting the macroscopic acoustic behavior of PU foam with high levels of impregnated GO.

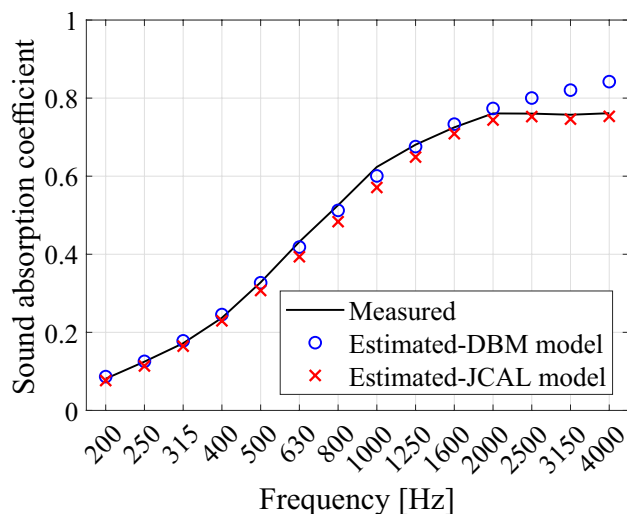


Fig. 16 Predicted absorption coefficients of GO4 derived from a model incorporating fully closed windows

5 Conclusion

We conducted a multiscale acoustic study of GO-impregnated PU foams. The PU foam underwent 1–4 GO impregnation cycles using a vacuum-assisted device, with the GO content increasing with each cycle. Measurements of the transport parameters revealed that GO impregnation markedly altered the macroscopic acoustic behavior of the PU foam. Particularly, a decrease in open porosity and increase in static airflow resistivity and tortuosity were observed. Consequently, the low-frequency absorption coefficient increased with increasing GO content, while the high-frequency absorption performance decreased. SEM imaging of the pristine and GO-impregnated PU foams revealed that the GO flakes covered the open pores. Quantification of the microstructural parameters confirmed that the opening ratio of the PU foam decreased due to GO impregnation. Utilizing the observed geometric parameters, Kelvin cell-type PUCs were constructed to perform microstructure-based acoustic simulations. For the pristine and low-GO-impregnated PU foams, models with partially open cells yielded excellent prediction accuracy for the transport parameters. Moreover, both the DBM and JCAL models proved effective in describing the macroscopic acoustic behavior. However, for PU foams with high GO contents, models with partially open cells resulted in lower accuracy, and failed to predict the decrease in open porosity attributable to the formation of closed pores by the impregnated GO. By integrating partially open and fully closed windows into the PUC model, we achieved a high congruence between the predicted and measured transport parameters. Furthermore, the JCAL model accurately predicted the macroscopic acoustic behavior. However, the DBM model, utilizing static airflow

resistivity as its sole input variable, was not suitable for predicting the high-frequency acoustic behavior. This limitation stems from the model's inability to account for the high tortuosity and low open porosity of PU foams with high concentrations of impregnated GO. This research advances our understanding of the acoustic characteristics of GO-impregnated PU foam and provides valuable insights for developing more effective sound-absorbing materials for noise control applications.

Acknowledgements This research was supported by the Institute of Engineering Research at Seoul National University and a grant from Kyung Hee University in 2020 (KHU-20201096).

Declarations

Conflict of interest The authors declare that they have no competing financial interests or personal relationships that may have influenced the work reported in this paper.

References

1. M.E. Delany, E.N. Bazley, Acoustical properties of fibrous absorbent materials. *Appl. Acoust.* **3**(2), 105–116 (1970). [https://doi.org/10.1016/0003-682X\(70\)90031-9](https://doi.org/10.1016/0003-682X(70)90031-9)
2. Y. Miki, Acoustical properties of porous materials-Modifications of Delany-Bazley models. *J. Acoust. Soc. Jpn. (E)* **11**(1), 19–24 (1990). <https://doi.org/10.1250/ast.11.19>
3. D.L. Johnson, J. Koplik, R. Dashen, Theory of dynamic permeability and tortuosity in fluid-saturated porous media. *J. Fluid Mech.* **176**, 379–402 (1987). <https://doi.org/10.1017/S0022112087000727>
4. Y. Champoux, J.F. Allard, Dynamic tortuosity and bulk modulus in air-saturated porous media. *J. Appl. Phys.* **70**, 1975–1979 (1991). <https://doi.org/10.1063/1.349482>
5. D. Lafarge, P. Lemarinier, J.F. Allard, V. Tarnow, Dynamic compressibility of air in porous structures at audible frequencies. *J. Acoust. Soc. Am.* **102**(4), 1995–2006 (1997). <https://doi.org/10.1121/1.419690>
6. J.G. Gwon, S.K. Kim, J.H. Kim, Sound absorption behavior of flexible polyurethane foams with distinct cellular structures. *Mater. Des.* **89**, 448–454 (2016). <https://doi.org/10.1016/j.matdes.2015.10.017>
7. R. Verdejo, R. Stämpfli, M. Alvarez-Lainez, S. Mourad, M.A. Rodriguez-Perez, P.A. Brühwiler, M. Shaffer, Enhanced acoustic damping in flexible polyurethane foams filled with carbon nanotubes. *Compos. Sci. Technol.* **69**, 1564–1569 (2009). <https://doi.org/10.1016/j.compscitech.2008.07.003>
8. S.H. Baek, J.H. Kim, Polyurethane composite foams including silicone-acrylic particles for enhanced sound absorption via increased damping and frictions of sound waves. *Compos. Sci. Technol.* **198**, 108325 (2020). <https://doi.org/10.1016/j.compscitech.2020.108325>
9. B.S. Kim, J. Choi, Y.S. Park, Y. Qian, S.E. Shim, Semi-rigid polyurethane foam and polymethylsilsesquioxane aerogel composite for thermal insulation and sound absorption. *Macromol. Res.* **30**(4), 245–253 (2022). <https://doi.org/10.1007/s13233-022-0026-8>
10. S.E. Samaei, U. Berardi, H.A. Mahabadi, P. Soltani, E. Taban, Optimization and modeling of the sound absorption behavior of polyurethane composite foams reinforced with kenaf fiber. *Appl.*

- Acoust. **202**, 109176 (2023). <https://doi.org/10.1016/j.apacoust.2022.109176>
11. J.M. Kim, D.H. Kim, J. Kim, J.W. Lee, W.N. Kim, Effect of graphene on the sound damping properties of flexible polyurethane foams. *Macromol. Res.* **25**(2), 190–196 (2017). <https://doi.org/10.1007/s13233-017-5017-9>
 12. J.H. Lee, I. Jung, Tuning sound absorbing properties of open cell polyurethane foam by impregnating graphene oxide. *Appl. Acoust.* **151**, 10–21 (2019). <https://doi.org/10.1016/j.apacoust.2019.02.029>
 13. J.H. Lee, J.H. Kim, Y.J. Shin, J.H. Jeon, Y.J. Kang, I. Jung, Multilayered graphene oxide impregnated polyurethane foam for ultimate sound absorbing performance: Algorithmic approach and experimental validation. *Appl. Acoust.* **203**, 109194 (2023). <https://doi.org/10.1016/j.apacoust.2022.109194>
 14. J.H. Oh, J.E. Kim, H.R. Lee, Y.J. Kang, I.K. Oh, Directionally antagonistic graphene oxide-polyurethane hybrid aerogel as a sound absorber. *ACS Appl. Mater. Interfaces* **10**(26), 22650–22660 (2018). <https://doi.org/10.1021/acsami.8b06361>
 15. J.H. Oh, H.R. Lee, S. Umrao, Y.J. Kang, I.K. Oh, Self-aligned and hierarchically porous graphene-polyurethane foams for acoustic wave absorption. *Carbon* **147**, 510–518 (2019). <https://doi.org/10.1016/j.carbon.2019.03.025>
 16. S.S. Yang, J.W. Lee, J.H. Kim, Y.J. Kang, Effect of thermal aging on the transport and acoustic properties of partially reticulated polyurethane foams. *J. Acoust. Soc. Am.* **152**(4), 2369–2381 (2022). <https://doi.org/10.1121/10.0014913>
 17. T.G. Zieliński, R. Venegas, C. Perrot, M. Červenka, F. Chevillotte, K. Attenborough, Benchmarks for microstructure-based modelling of sound absorbing rigid-frame porous media. *J. Sound Vib.* **483**, 115441 (2020). <https://doi.org/10.1016/j.jsv.2020.115441>
 18. Y. Salissou, R. Panneton, Pressure/mass method to measure open porosity of porous solids. *J. Appl. Phys.* **101**, 124913 (2007). <https://doi.org/10.1063/1.2749486>
 19. Z.E.A. Fellah, S. Berger, W. Lauriks, C. Depollier, C. Aristegui, J.-Y. Chapelon, Measuring the porosity and the tortuosity of porous materials via reflected waves at oblique incidence. *J. Acoust. Soc. Am.* **113**, 2424–2433 (2003). <https://doi.org/10.1121/1.1567275>
 20. ASTM C522-03: Standard Test Method for Airflow Resistance of Acoustical Materials (ASTM International, West Conshohocken, PA, 2016)
 21. L. Jaouen, E. Gourdon, P. Glé, Estimation of all six parameters of Johnson-Champoux-Allard-Lafarge model for acoustical porous materials from impedance tube measurements. *J. Acoust. Soc. Am.* **148**(4), 1998–2005 (2020). <https://doi.org/10.1121/10.0002162>
 22. S.F. de Sá, J.L. Ferreira, A.S. Matos, R. Macedo, A.M. Ramos, A new insight into polyurethane foam deterioration—the use of Raman microscopy for the evaluation of long-term storage conditions. *J. Raman Spectrosc.* **47**, 1494–1504 (2016). <https://doi.org/10.1002/jrs.4984>
 23. J.H. Park, K.S. Minn, H.R. Lee, S.H. Yang, C.B. Yu, S.Y. Pak, C.S. Oh, Y.S. Song, Y.J. Kang, J.R. Youn, Cell openness manipulation of low density polyurethane foam for efficient sound absorption. *J. Sound Vib.* **406**, 224–236 (2017). <https://doi.org/10.1016/j.jsv.2017.06.021>

Publisher's Note Springer Nature remains neutral with regard to jurisdictional claims in published maps and institutional affiliations.

Springer Nature or its licensor (e.g. a society or other partner) holds exclusive rights to this article under a publishing agreement with the author(s) or other rightsholder(s); author self-archiving of the accepted manuscript version of this article is solely governed by the terms of such publishing agreement and applicable law.

Authors and Affiliations

Sung Soo Yang¹ · Inhwa Jung² · Yeon June Kang¹

✉ Inhwa Jung
ijung@khu.ac.kr

✉ Yeon June Kang
yeonjune@snu.ac.kr

¹ Institute of Advanced Machines and Design, School of Mechanical Engineering, Seoul National University, Seoul, Republic of Korea

² Department of Mechanical Engineering, Kyung Hee University, Yongin, Republic of Korea